Optics and Laser Technology

Controlling the shell thickness of SiO2 on TiO2 NPs: Characterization, linear and nonlinear optical properties

--Manuscript Draft--

Manuscript Number:	JOLT-D-23-04068
Article Type:	Research Paper
Section/Category:	Optical Materials-Thin films
Keywords:	Nanoparticles; Sol-gel; TiO2@SiO2 core/shell; TEM; Refractive index; Wemple-DiDomenico model
Corresponding Author:	Tarek Soliman Ural Federal University named after the first President of Russia B N Yeltsin Institute of Natural Sciences and Mathematics Ekaterinburg, RUSSIAN FEDERATION
First Author:	Tarek Soliman
Order of Authors:	Tarek Soliman
	Ahmed Khalid
	A. Farid
	Mohamed Taha
	S. Abdallah
Abstract:	TiO2 nanoparticles (NPs) were prepared by the sol-gel method and then encapsulated with different thicknesses of SiO2 as a shell using the Stöber method. The crystal, chemical structure, and morphology of the core-shell TiO2@SiO2 NPs were characterized using XRD, FTIR, and TEM techniques. The amorphous nature of the shell (SiO2) was shown by XRD examination, which influenced the crystallinity of the TiO2 NPs, while FTIR data verified the association between SiO2 and TiO2, and a TEM study validated the coating of TiO2 NPs with SiO2. The optical absorption of TiO2 NPs was characterized by a sharp absorption edge around 343 nm, which redshifted to a higher wavelength region with increasing shell thickness. The direct bandgap was found to decrease from 3.97 eV for TiO2 to about 3.60, 3.37, and 3.26 eV for TiO2@SiO2, with shell thicknesses of about 2.5, 5.5, and 8 nm, respectively. The refractive index and extinction coefficient increased with increasing shell thickness. Furthermore, an enhancement in the optical conductivity of TiO2 NPs was observed with increasing shell thickness. The Wemple-DiDomenico model was applied to compute the nonlinear refractive index (n2), first- and third-order (c(1) & c(3)) susceptibilities values. An enhancement was observed for all nonlinear optical parameters with the insertion of the shell SiO2 into the core TiO2. The value of (c(3)) was increased from 2.08´10-14 for pure TiO2 NPs to 3.04´10-09 for the core-shell TiO2@SiO2 sample with a shell thickness of 8 nm.
Suggested Reviewers:	R.k. manavalan r.k.manavalan@urfu.ru
	Ram Jeewan Sengwa rjsengwa@rediffmail.com
	Hesham MH Zakaly h.m.zakaly@gmail.com

To

The Editor-in-Chief

Subject: Submission of a manuscript for evaluation

Dear Editor,

According to your journal scope, I would like to submit the attached manuscript entitled **"Controlling the shell thickness of SiO_2 on TiO_2 NPs: Characterization, linear and nonlinear optical properties"** for consideration for possible publication in your journal. With the submission of this manuscript, I would like to undertake that above mentioned manuscript has not been published elsewhere, accepted for publication elsewhere or under editorial review for publication elsewhere.

Thank you in advance.

Sincerely yours

Corresponding authors:

***T.S. Soliman**

Tarek.attia@fsc.bu.edu.eg

Highlights

1. Core-shell TiO_2@SiO_2 nanoparticles with different shell thicknesses were synthesized using the Stöber method.
2. The impact of the silica shell thickness on the structural and optical properties of TiO_2 was investigated.
3. Linear and non-linear optical parameters of TiO_2 and TiO_2@SiO_2 with different shell thickness were investigated.

Controlling the shell thickness of SiO_2 on TiO_2 NPs: Characterization, linear and nonlinear optical properties

Mohamed Taha[1], A. Khalid [2], A. Farid[1,3], S. Abdallah [2], T.S. Soliman [4, 5, *]

[1]Nano Gate, 9254 Hodashaarawy, Al Abageyah, El Mukkatam, Cairo 43511, Egypt

[2]Department of Basic Engineering Sciences, Faculty of Engineering (Shoubra), Benha University, Benha, Egypt

[3]Central Metallurgical Research and Development Institute (CMRDI), Cairo, Egypt

[4] Institute of Natural Sciences and Mathematics, Ural Federal University, Ekaterinburg 620000, Russian Federation

[5]Physics Department, Faculty of Science, Benha University, Benha 13518, Egypt

*Corresponding author E-mail: tarek.attia@fsc.bu.edu.eg

Abstract

TiO_2 nanoparticles (NPs) were prepared by the sol-gel method and then encapsulated with different thicknesses of SiO_2 as a shell using the Stöber method. The crystal, chemical structure, and morphology of the core-shell TiO_2@SiO_2 NPs were characterized using XRD, FTIR, and TEM techniques. The amorphous nature of the shell (SiO_2) was shown by XRD examination, which influenced the crystallinity of the TiO_2 NPs, while FTIR data verified the association between SiO_2 and TiO_2, and a TEM study validated the coating of TiO_2 NPs with SiO_2. The optical absorption of TiO_2 NPs was characterized by a sharp absorption edge around 343 nm, which redshifted to a higher wavelength region with increasing shell thickness. The direct bandgap was found to decrease from 3.97 eV for TiO_2 to about 3.60, 3.37, and 3.26 eV for TiO_2@SiO_2, with shell thicknesses of about 2.5, 5.5, and 8 nm, respectively. The refractive index and extinction coefficient increased with increasing shell thickness. Furthermore, an enhancement in the optical conductivity of TiO_2 NPs was observed with increasing shell thickness. The Wemple-DiDomenico model was applied to compute the nonlinear refractive index (n_2), first- and third-order ($\chi^{(1)}$ & $\chi^{(3)}$) susceptibilities values. An enhancement was observed for all nonlinear optical parameters with the insertion of the shell SiO_2 into the core TiO_2. The value of ($\chi^{(3)}$) was increased from 2.08×10^{-14} for pure TiO_2 NPs to 3.04×10^{-09} for the core-shell TiO_2@SiO_2 sample with a shell thickness of 8 nm.

Keywords: Nanoparticles; Sol-gel; TiO_2; TiO_2@SiO_2 core/shell; Refractive index; Wemple–DiDomenico model.

1. Introduction

Recently, there has been growing interest in the development of nanomaterials for biomedical applications due to their unique properties and potential for enhancing diagnostic and therapeutic approaches [1-6]. Among these nanomaterials, core-shell nanoparticles (NPs) have emerged as a promising platform for various biomedical applications [7-10]. In particular, core-shell TiO_2@SiO_2 NPs have attracted significant attention due to their combined properties and versatile applications in the field of biomedicine [11-14]. The core of these NPs is composed of metal oxide nanocrystalline semiconductive materials, particularly titanium dioxide (TiO_2), known for its excellent photocatalytic and optical properties [14-18]. TiO_2 NPs exhibit high photostability [19,20] and have attracted significant attention across various fields due to their vast potential in photocatalysis [21-24], solar cells [25-27], nonlinear optics [28-31] and sensors [32-35]. Due to the chemical and electrostatic stability of silica, it can operate as a protective shell to limit contact with the surrounding media after coating the nanoparticles [36]. Lately, SiO_2 has been coated with a shell from TiO_2 and found to enhance the scattering efficiency in dye-sensitized solar cell applications and show enhanced power conversion efficiency [37]. Furthermore, there are many limitations to use bare TiO_2 nanoparticles in biological systems due to their potential cytotoxicity and lack of stability in physiological conditions [38-42]. To overcome these limitations, a silica (SiO_2) shell is applied as a protective coating around the TiO_2 core. The SiO_2 shell provides biocompatibility, stability, and surface functionalization capabilities to the nanoparticles. The biocompatible nature of SiO_2 allows for the safe use of core-shell TiO_2@SiO_2 in biological environments, reducing the risk of adverse effects on cells and tissues [40, 43-45]. Moreover, the SiO_2 shell offers opportunities for surface modification with various functional groups, biomolecules, or targeting ligands. This surface functionalization enables specific targeting and interaction with biological entities, such as cells, tissues, or biomarkers, making core-shell TiO_2@ SiO_2 NPs versatile tools for targeted drug delivery, bio-imaging, and sensing applications [45-49]. Furthermore, the unique optical properties of core-shell TiO_2@SiO_2 NPs, including light absorption and emission, make them excellent candidates for photodynamic therapy with improvement of biocompatibility [50,51]. They can be utilized as contrast agents in various imaging modalities, including fluorescence imaging, photoacoustic imaging, and computed tomography (CT), allowing for real-time monitoring and visualization of biological processes [52-54].

Core-shell TiO_2@SiO_2 synthesis poses a significant challenge, with preparation methods categorized into liquid-solid [46, 55] and gas-solid transformations [46, 56]. Among these methods, the sol-gel technique stands out as a widely used and cost-effective approach for material preparation. It offers several advantages, including easier control over chemical compositions, morphology, and crystallite size of the nanomaterial [14, 46]. Additionally, the sol-gel technique ensures compositional homogeneity, enabling precise regulation of structural morphology and grain size [40, 57, 58].

Herein, a straightforward technique for synthesizing TiO_2@SiO_2 core-shell was presented with control of silica shell thickness. Three different thicknesses of the shell were obtained and its impact on the structure and optical properties of TiO_2 NPs was investigated. Changes in structure and morphology were assessed using XRD, FTIR, and TEM techniques. With the use of UV-visible data, the optical properties of the TiO_2@SiO_2 nanocomposite were evaluated.

2. Experimental and procedure

2.1. Materials and chemicals

Titanium (IV) isopropoxide (TTIP) and Tetraethoxysilane (TEOS, ≥99.0%) were purchased from Sigma-Aldrich, Germany. Isopropanol (IPA) was obtained from Chem-Lab Analytical based in Belgium. Merck in Darmstadt, Germany provided ammonia aqueous solution (25%), Absolute ethanol (99.5%), and nitric acid (69%). All compounds were of reagent quality and were utilized as supplied, with no extra purification required.

2.2. TiO_2 Nanoparticles preparation

TiO_2 NPs were produced using sol–gel technique according to the procedure previously mentioned [30]. Titanium (IV) isopropoxide (TTIP) was dissolved in isopropanol, resulting in the rapid formation of a transparent stock solution. The stock solution was carefully added in small droplets to deionized water while vigorously stirring at room temperature, leading to the formation of a white gel. The solution was subsequently treated with a 1M nitric acid solution until the pH value reached 2 and then maintained at a temperature of 70°C for duration of 24 hours.

2.3. Synthesis of TiO_2-SiO_2 core-shell nanoparticles

The Stöber method was used to synthesize TiO_2@SiO_2 core-shell [38]. The specific procedure involved several steps. Initially, a mixture of 10 ml deionized water and 100 ml

ethanol was prepared, to which 1 g of TiO_2 was added. Then, for 30 minutes, the mix was subjected to ultrasonics to disperse the TiO_2 particles. In the subsequent stage, different concentrations of TEOS (Tetraethyl orthosilicate) were sequentially introduced into the suspension. The TEOS concentrations used were 0.099M, 0.19M, and 0.28M. Additionally, ammonia was added gradually, aiming to attain the desired pH level of 10. This addition of ammonia was carried out under continuous stirring. The resulting mixture was vigorously stirred at 20°C for 12 hours to allow for a complete reaction. Following a 12-hour stirring period, the mixtures underwent centrifugation at 7500 rpm/5 minutes. The liquid phase was carefully removed, leaving behind the resulting silica coated TiO_2 NPs. To eliminate any excess reactants, the nanoparticles were subjected to three washes with ethanol. Subsequently, the particles were dried overnight at 100 ˚C. The denotation given to the resulting silica coated TiO_2 nanoparticles was TSM, where M represents different concentrations of TEOS. Specifically, M was assigned values of 1, 2, and 3, corresponding to TEOS concentrations of 0.099M, 0.19M, and 0.28M (TS1, TS2, and TS3), respectively. The reaction process is visually depicted in Fig. 1.

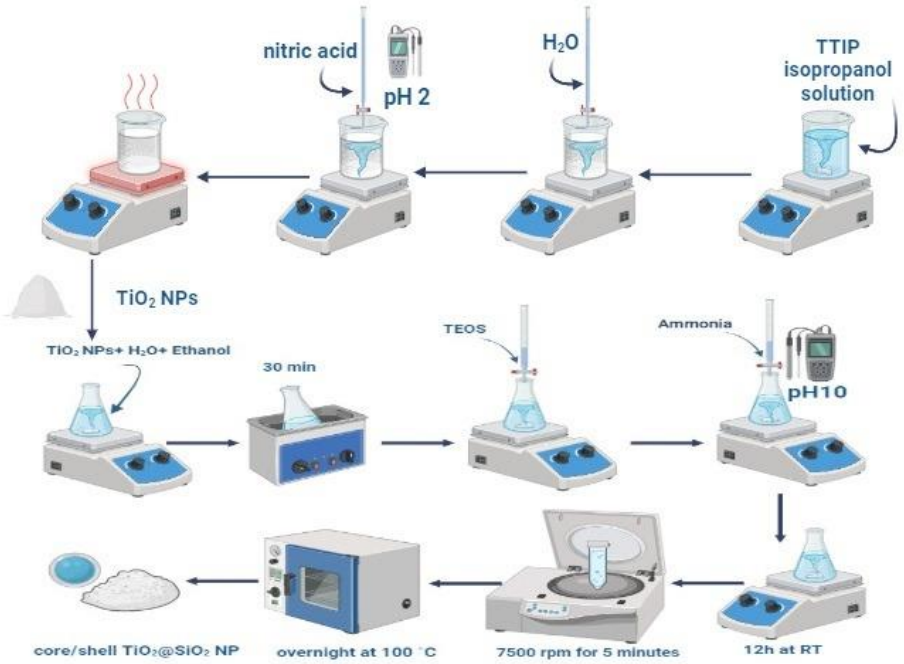

Fig. 1: visual representation of the synthetic pathway utilized to generate core-shell TiO_2@SiO_2 NPs.

2.4. Material Characterization

The X-ray powder diffraction (XRD) technique was performed using the XPERT-PRO to record the crystal structures of the prepared samples. The XRD measurements were conducted

over a range of 5° ≤ 2θ ≤ 90°, with a minimum step size of 2θ: 0.001, and at wavelength (Kα) = 1.54614°. The morphological characteristics of the produced TiO_2 powder and synthesized TiO_2@SiO_2 core-shell powder was examined using transmission electron microscopy (TEM) with Talos F-200i (Thermo-Scientific) high-resolution TEM operating at an accelerating voltage of 200 kV. To investigate the various chemical bonds presented in the prepared samples, FT-IR vertex 70 RAM II, Bruker was utilized. FTIR spectra were collected at room temperature, covering a 400-4000 cm^{-1} range. A double-beam spectrophotometer (Perkin Elmer Lambda 40) was used to analyze the UV-visible absorption spectra of materials.

3. Results and discussions

3.1. Characterization

3.1.1. XRD analysis

XRD analysis was performed to validate the crystal structure of the prepared nanoparticles. **Fig. 2** presents the XRD patterns of TiO_2 and TiO_2@SiO_2 NPs.

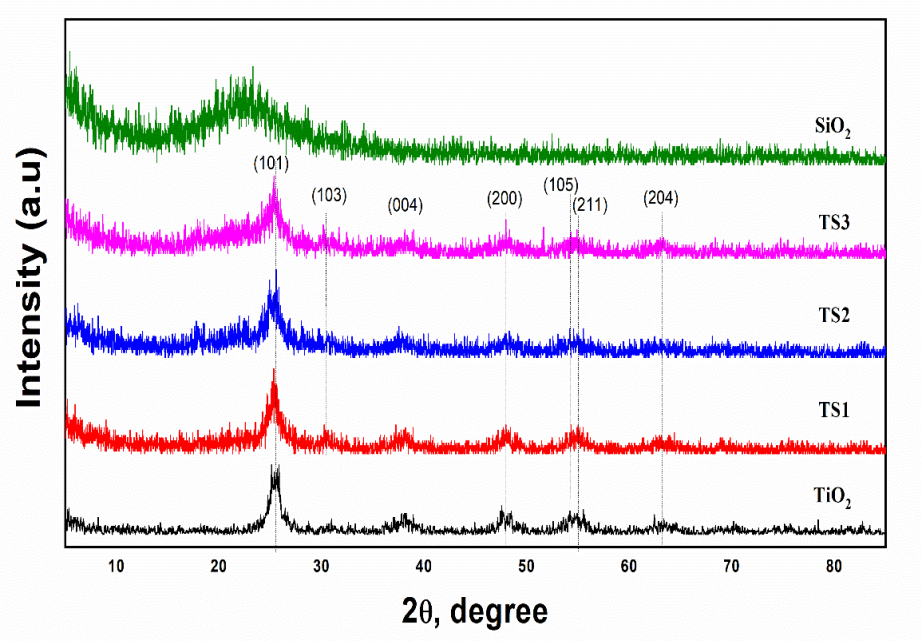

Fig.2: XRD patterns for prepared samples.

The TiO_2 pattern coincides with anatase TiO_2 (JCPDS No. 01-075-2552), with no diffraction peaks correlated to the TiO_2-polymorphs identified. Specifically, the peaks at 25.335°, 36.98°, 37.809°, 48.104°, 53.92°, 55.138° and 62.752° corresponded to the (101), (103), (004), (200),

(105) and (211) and (204) planes of anatase TiO_2, respectively [59]. For pure silica NPs, a broad peak was observed around 22° was assigned to the silica amorphous structure. Diffraction patterns obtained from TiO_2@SiO_2 core-shell prepared with different TEOS concentrations further demonstrated the influence of TEOS on the crystallinity of the composite. In these patterns, the diffraction background of TS1, TS2, and TS3 wasn't a flat-line at $2\theta = 25.335°$ but instead displayed broadband. This was attributed to the presence of amorphous SiO_2 on the surface of the nanocrystalline TiO_2 [60, 61]. Moreover, as the TEOS concentration increases, the peak intensity in TS1, TS2, and TS3 becomes weaker and broader, indicating lessened crystallinity [60]. Furthermore, the increase in TEOS concentration promotes the formation of a thicker and more continuous SiO_2 shell around the TiO_2 core and induces the formation of amorphous regions within the composite, which results in a broad peak in the XRD spectra [62].

3.1.2. Transmission electron microscope analysis

HR-TEM was used to identify the morphology and size of the core TiO2 and the shell thickness SiO2, as shown in Fig. 3. The TEM images, specifically Fig. 3a & b, confirmed that TiO_2 NPs exhibited a spheroidal shape with an average particle size of 3.45 nm, as illustrated by the corresponding histogram (Fig. 3c). For TS1, TS2 and TS3 a clear contrast was observed suggesting that formation of a shell layer from amorphous SiO_2 around TiO_2 NPs. Briefly, TEM images of TS1 were displayed in Fig. 3(d, e, and f) having an average size of around 5:6.4 nm with shell thickness ~ 2.5 nm. Whereas TEM images for TS2 shown in Fig. 3(g, h, and I) presented an average size ranging from 9:12 nm with a shell layer of about ~5.5 nm. Furthermore, TEM images of TS3 are shown in Fig. 3(j, k, and l). The coated particles displayed a size range of 12:15 nm, with a SiO_2 thickness around ~ 8nm. The HR-TEM of TS3, Fig.3m, showed d-spacing of 0.35 nm that corresponding to (101) plane of the TiO_2-anatase.

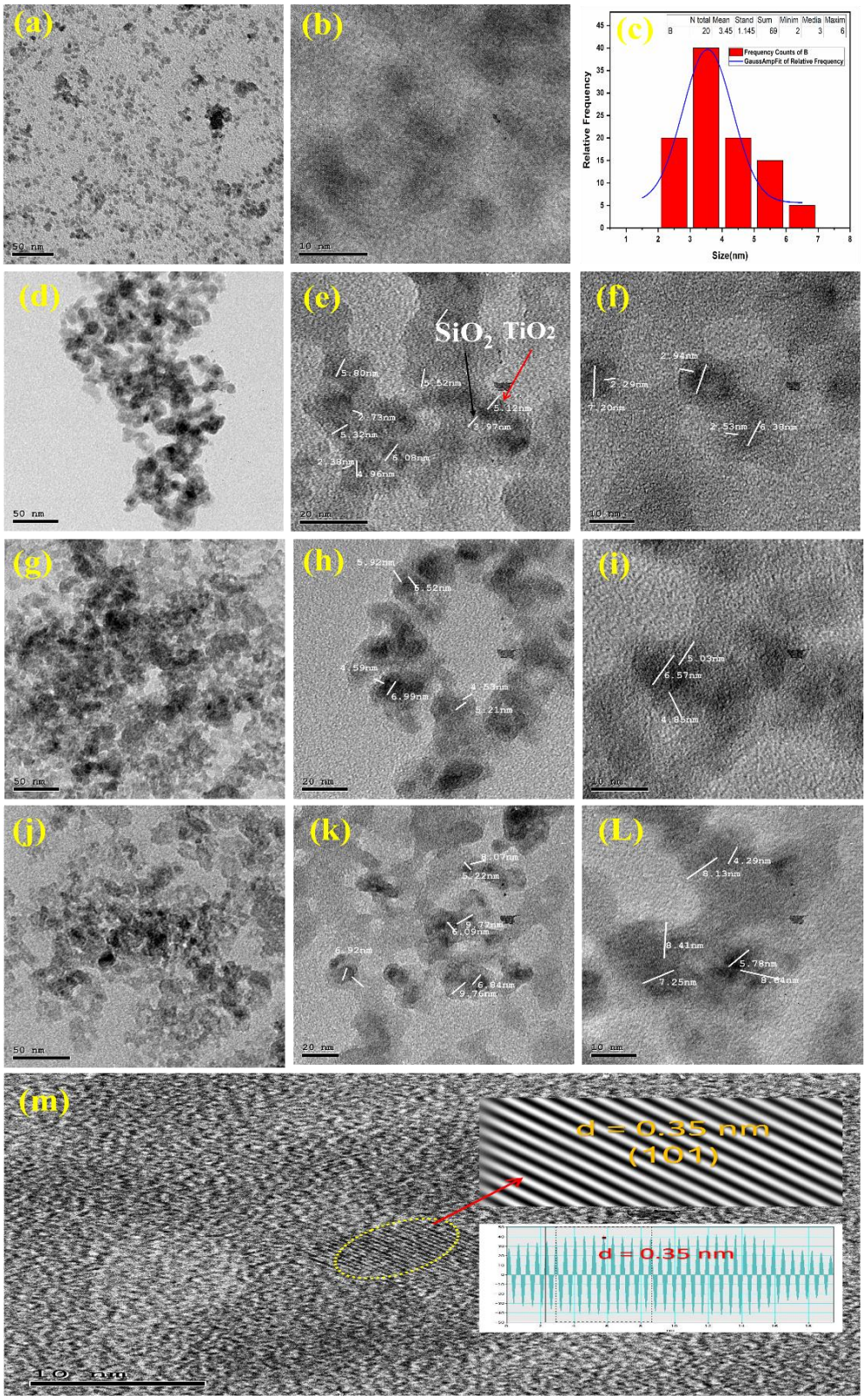

Fig.3: TEM images for; (a, b, & c) TiO_2, (d, e, & f) TS1, (g, h, & i) TS2, (j, k, & l) TS3, and (m) HR-TEM for TS3.

3.1.3. FT-IR analysis

FTIR spectra were conducted on the SiO_2, TiO_2, TS1, TS2, and TS3 samples, as depicted in Fig. 4., pure SiO_2 displayed strong absorption peaks at approximately 1069.15 and 978.8 cm^{-1} corresponding to the symmetric Si-O-Si bending vibration. Additionally, the absorption bands at 804.57 and 451.95 cm^{-1} are assigned to Si-O-Si asymmetric stretching vibrations[68]. For pure TiO_2, the bands in the region from 400 to 800 cm^{-1} are assigned to Ti-O vibration[69], and the de-formative vibration of Ti-OH stretching mode was observed at 1631.70 cm^{-1} [70]. For composite structures, a weak absorption band at 954.42 cm^{-1} in TS1 is attributed to Si-O-Ti flex vibrations, which testifies to the chemical bond between TiO_2 and SiO_2 [63, 64]. Furthermore, this band was shifted to 956.13 and 957.31 cm^{-1} for TS2 and TS3, respectively, indicating the variation in shell thickness for the three composites. FT-IR bands revealed that these absorption peaks were generally more pronounced in the coated TiO_2 samples with higher silica content. This strongly suggests the encapsulation of TiO_2 NPs within the silica matrix [65, 66]. Furthermore, absorption bands in the range of 800–400 cm^{-1}, corresponding to the characteristic vibrational modes of Ti-O of TiO_2, were observed, indicating the presence of the core-TiO_2 structure [38, 67]. Such a result is predicted to have a noticeable impact on the optical properties of the TiO_2 NPs.

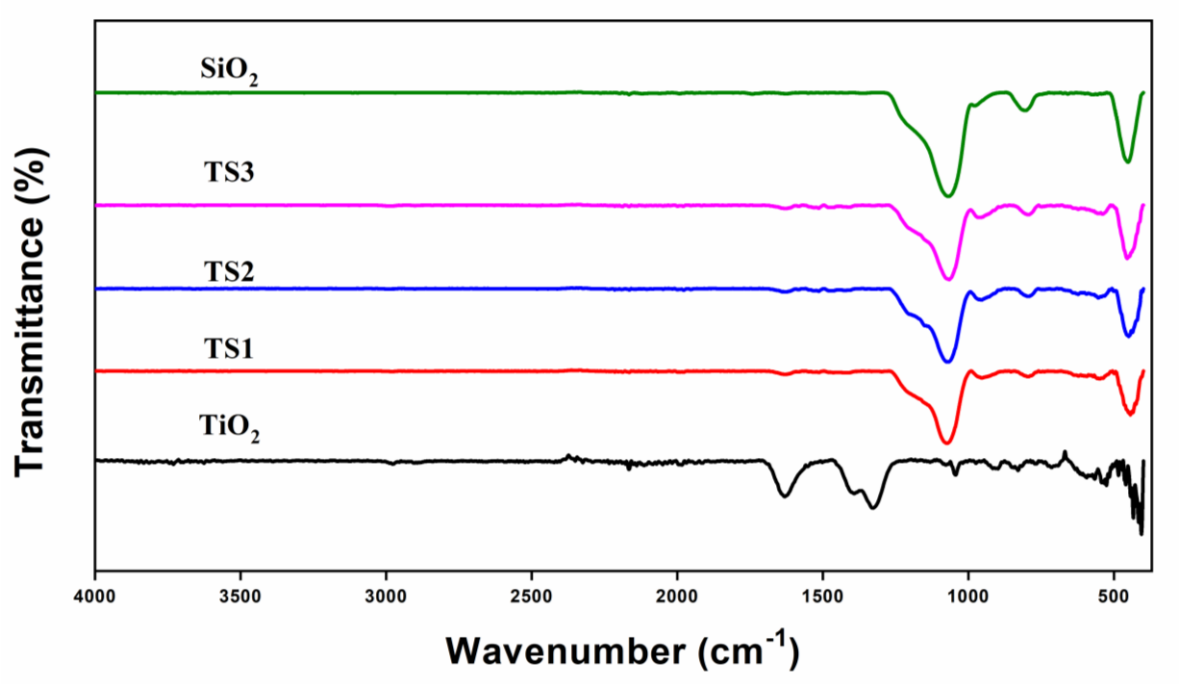

Fig.4: FTIR patterns for prepared samples.

3.2 Optical features

3.2.1 UV-visible spectra, optical bandgap, and linear refractive index

The TiO_2@SiO_2 core-shell absorption spectra with different thickness of the SiO_2 shell are shown in Fig.5. The absorption spectrum of the pure TiO_2 NPs shows an absorption edge around a 343 nm range (Fig.5a). Encapsulation of the TiO_2 surface by the silica shell leads to increased absorption intensity and redshift in absorption edge to about 387, 445, and 482 nm for TiO_2@SiO_2 with shell thickness 3, 6, and 9 nm, respectively (Fig.5b). In addition, the shift increases to a higher wavelength region with increasing the thickness of the SiO_2 shell as shown in Fig.5b. This finding increases the efficiency with which simulated sunlight is used in solar cell and photocatalysis applications.

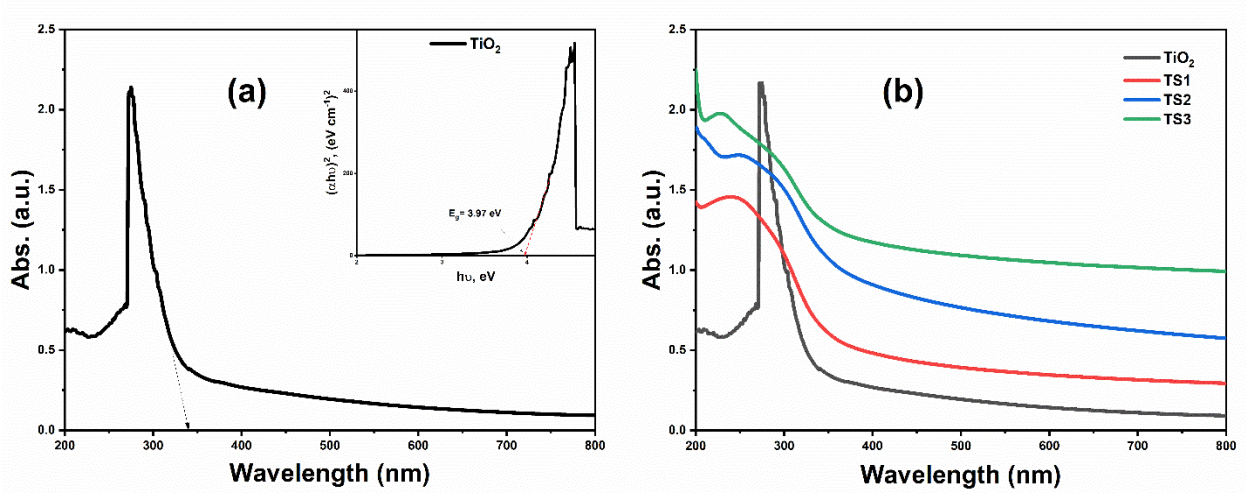

Fig.5: The absorbance as a function of wavelength for prepared samples.

The redshift in the absorption spectra is caused because of the quantum confinement effect. As shown in the TEM analysis the SiO_2 shell increases in size with increasing the TEOS concentration during the reaction process. This increase in particle size causes a redshift in the absorption spectra, and the electronic transition structure of the material changes in accordance. This change was discussed with the help of Tauc's relation as follows [71];

$$(\alpha h\upsilon)^2 = A(h\upsilon - E_{gd}) \quad (1)$$

$$(\alpha h\upsilon)^{1/2} = A(h\upsilon - E_{gi}) \quad (2)$$

where E_{gd} and E_{gi} are the direct and indirect bandgap energies, respectively. Fig.6 shows the relation of $(\alpha h\upsilon)^2$ and $(\alpha h\upsilon)^{1/2}$ as a function of $(h\upsilon)$. The E_{gd} and E_{gi} values are extracted in Table 1.

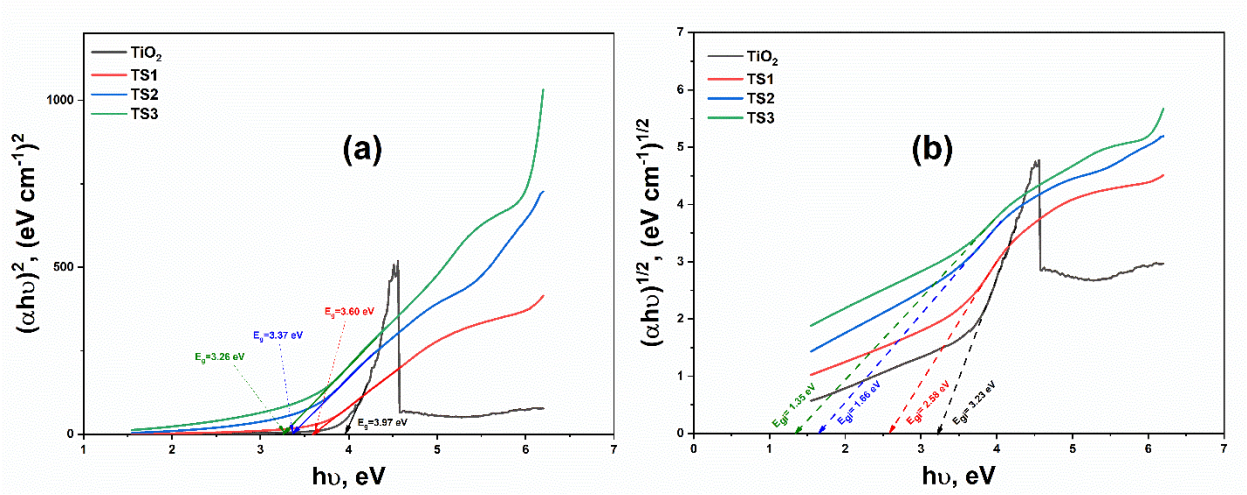

Fig.6: Plots of (a) (α hυ)^2 and (b) (α hυ)$^{1/2}$ vs. (h υ) of the prepared samples.

as shown in Table 1, E_{gd} and E_{gi} values decreased dramatically with increasing the shell thickness. Herein, the E_{gd} value of the pure TiO_2 is higher than that of the bulk TiO_2 (3.2 eV), which could be caused by the tiny size of the TiO_2 NPs (3 nm) compared to that present in the literature [72-75]. The particle size of TiO_2 is about 3 nm, and the shell varies from 3 to 9 nm, so the quantum confinement effect is expected, and the absorption edge shifts to a higher wavelength with increasing particle size [73]. Furthermore, the insertion of SiO_2, as a shell, on the TiO_2 core creates defects and causes the absorption edge to be redshifted, and the bandgap decreases accordingly. Decreasing the bandgap makes the prepared samples possible candidates in photovoltaic applications. Raising the defects and the disorder in the electronic levels of the materials could be proved by measuring the band tail width in the forbidden region through the following relation [71];

$$\alpha = \alpha_0 e^{[\frac{h\upsilon}{E_U}]} \qquad (3)$$

where α_0 is constant and E_U is the band-tail width or Urbach energy. The E_U value was investigated through the linear relation between ln(α) on Y-axis and (hυ) on X-axis (Fig.7). From Table 1, the increase in the E_U value indicates the increase in the disordering of the material and the increase of localized states in the forbidden region caused by the produced defects due to the insertion of SiO_2.

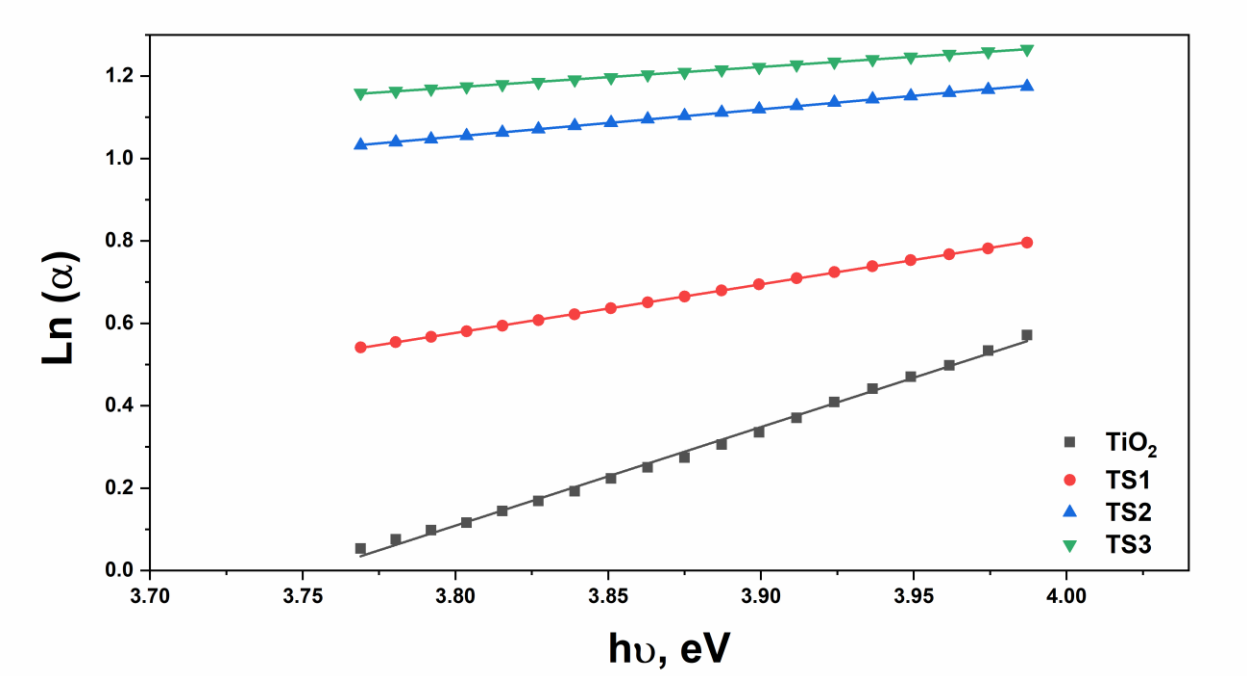

Fig.7: ln(α) against hυ of the prepared samples.

Table 1: Optical bandgaps and Urbach energy for prepared samples.

nanocomposite ID	E_{gd} (eV)	E_{gi} (eV)	E_U (eV)	*n*(λ=500nm)
TiO_2	3.97	3.23	0.42	2.052
TS1	3.60	2.58	0.85	2.809
TS2	3.37	1.66	1.52	4.359
TS3	3.26	1.35	2.02	5.979

The refractive index (n) and the extinction coefficient (k) are related to the materials' reflectivity and attenuation or absorption coefficient, respectively, and are two of the most essential optical factors. Both factors are related to each other through the following relations [71];

$$n = \frac{1-R}{1+R} + \sqrt{\frac{4R}{(1-R)^2} - k^2} \qquad (4)$$

$$k = \frac{\alpha\lambda}{4\pi} \qquad (5)$$

The reflectance ($R = 1 - \sqrt{T * e^{A}}$) was investigated through the absorption (A) and transmission (T) data obtained from the UV-visible spectra. As a function of the incident light wavelength, the n and k dependencies are represented in Fig. 8.

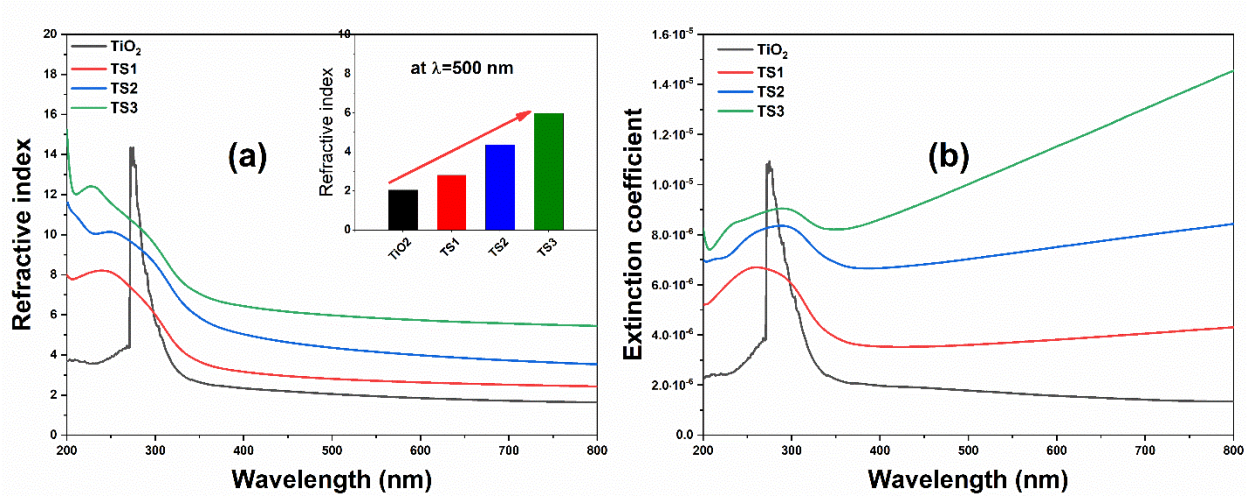

Fig.8: Plots of (a) Refractive index and (b) extinction coefficient as a function of wavelength for prepared samples.

It was shown that *n* increases with increasing the thickness of the shell SiO_2, as illustrated in the inset of Fig.8a. Moreover, in the UV region (200 ≤ λ≤ 300 nm), n has a higher value due to the resonance effect, which is caused by the interaction of the incoming electromagnetic-radiation and the electrons polarization, as the incident photons frequency becomes equal to the plasma frequency [76, 77]. Thus, the refractive index exhibits anomalous dispersion in this region. Moving towards the visible region (400 ≤ λ≤ 800 nm), the value of n decreases exponentially. However, at higher wavelengths, the decrease in *n* value is slight and appears to remain constant. The absorption of the electromagnetic waves became less, and most of the incident energy was reflected. As shown in Fig.8b, based on this data, it appears that *k* decreases as the wavelength of incident photons increases, and seems constant for the pure TiO_2 NPs sample in the visible region. The k value then begins to rise with the insertion of SiO2, rises with the growth in shell thickness, and rises significantly at the highest shell thickness. The high value of the refractive index makes it useful as an anti-reflective coating in solar cell devices.

3.2.2. Optical dielectric constants

Optical dielectric constants, real (ε′) and imaginary (ε′′) parts, depend on the n and k values of the material which can be determined through the following relations [71];

$$\varepsilon' = n^2 - k^2 \quad (6)$$

$$\varepsilon'' = 2nk \quad (7)$$

The dependences of both factors, ε′ and ε′′, on the incident photon energy are illustrated in nFig.9. obviously ε′ and ε′′ increases with increasing the shell thickness.

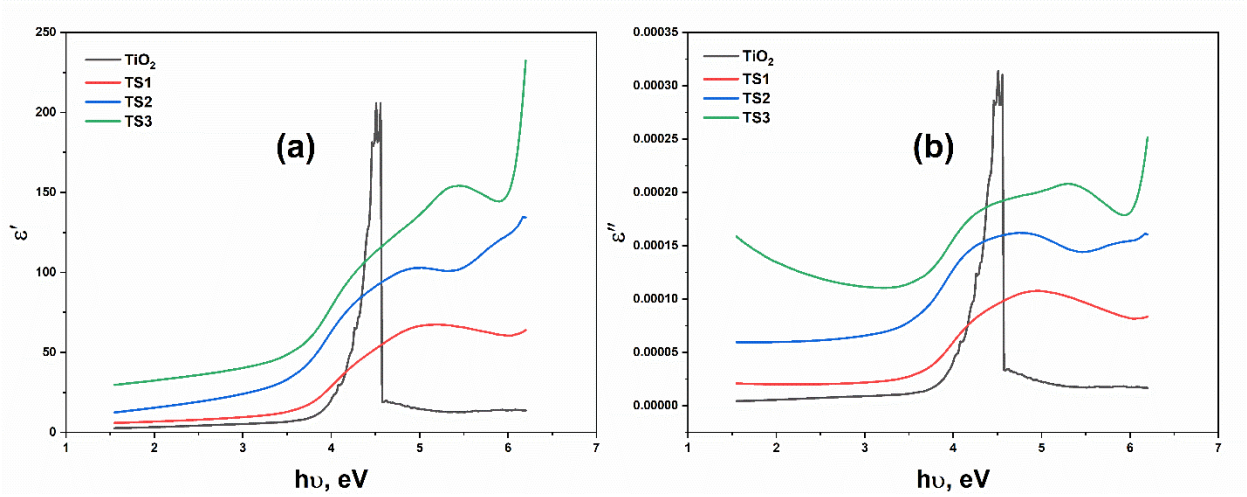

Fig.9: Plots of (a) ε′ and (b) ε″ vs. hυ for prepared samples.

The similarity between the behavior of the ε′ with refractive index and ε″ with *k* is evident. Moreover, ε′ value is larger than that for ε″. Increasing the shell thickness causes a change in polarization, resulting in high ε′ and low ε″ values and less energy dissipation.

Optical conductivity ($\sigma_{opt.}$) is dependent upon various factors such as α, *n*, and the frequency of incident photons through the following relation [77]:

$$\sigma_{opt.} = \frac{\alpha n c}{4\pi} \quad (8)$$

where ($c=3\times10^8$ m/sec) is the speed of light in free space. Fig.10 depicts the correlation between the energy of incoming photons and $\sigma_{opt.}$. It can be observed that as the shell thickness increases the $\sigma_{opt.}$ increases. This might be due to the increase in α and *n* values of the material with increasing shell thickness. At high photon energies, optical conductivity is enhanced due to the excitation of electrons by incident photons. The $\sigma_{opt.}$ value of TiO_2 NPs at 600 nm is about

$1.45x10^9$ sec^{-1} which increases to about 5.01 $x10^9$, $1.5x10^{10}$, and $3.31x10^{10}$ sec^{-1} for the core-shell TiO_2@SiO_2 with different shell thickness TS1, TS2, and TS3, respectively.

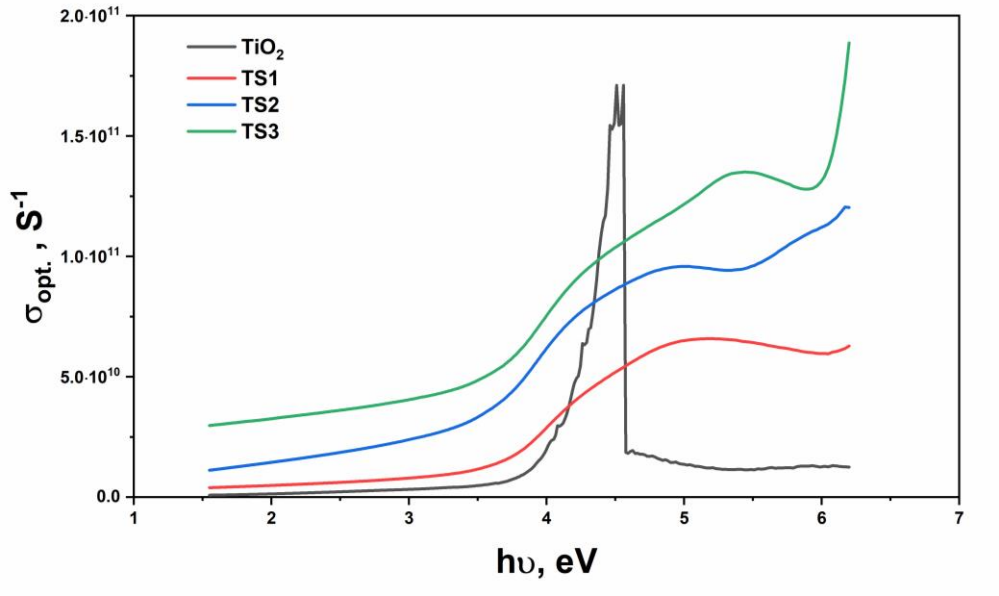

Fig.10: The variation of $\sigma_{opt.}$ with (h υ) of the prepared samples.

3.2.3. Dispersion energy parameters

The dispersion energy is a significant factor in researching optical materials for spectral dispersion and visual communications. The analysis of refractive index dispersion has been conducted by implementing the single oscillator concept using the Wemple-DiDomenico relationship, which depends on the dispersion-energy (E_d) and the oscillator-energy (E_0) as follows [78, 68]:

$$\frac{1}{(n^2-1)} = \frac{E_0}{E_d} - \left(\frac{1}{E_0 E_d}\right)(h\upsilon)^2 \qquad (9)$$

Plot of $1/(n^2 - 1)$ versus $(h\upsilon)^2$ is illustrated in Fig. 11. From the slope and the intercept values, we can derive the values of E_d and E_0 (Table 2).

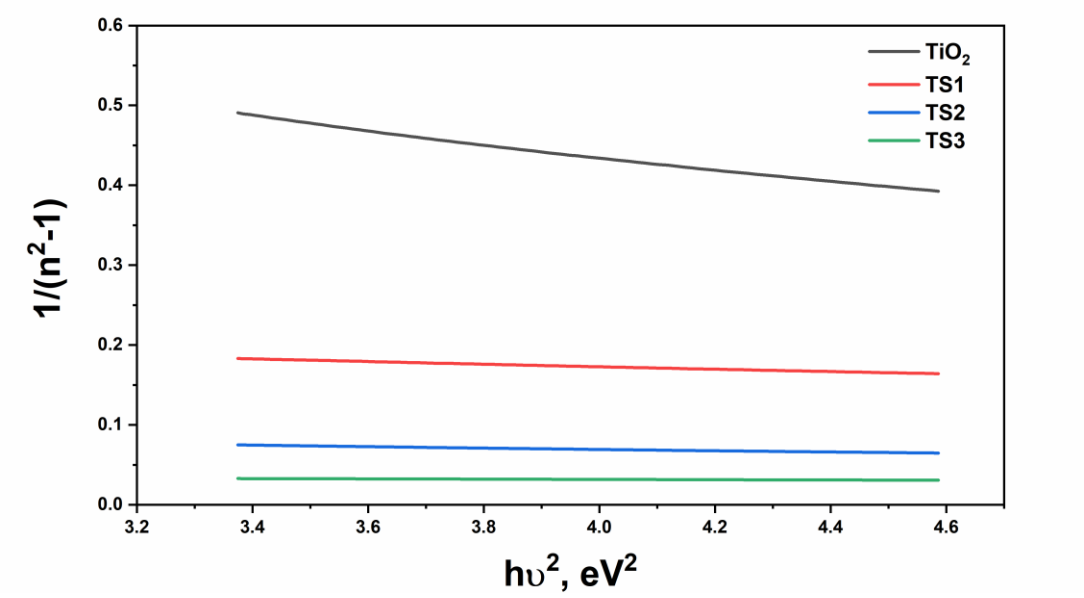

Fig.11: $1/(n^2-1)$ vs. $(h\upsilon)^2$ for the prepared samples.

Table 2: The optical dispersion parameters of the TiO_2 and TiO_2@SiO_2 core-shell.

Sample ID	E_d(eV)	E_0(eV)	*f*, eV^2	n_0	$\varepsilon_s=n_0^2$	$\chi^{(1)}$ (esu)	$\chi^{(3)}$ (esu)	n_2 (esu)
TiO_2	4.06	3.07	12.45	1.523	2.32	0.11	2.08×10^{-14}	5.14×10^{-13}
TS1	16.40	3.87	63.49	2.289	5.24	0.34	2.20×10^{-12}	3.62×10^{-11}
TS2	34.02	3.50	119.19	3.272	10.71	0.77	6.06×10^{-11}	6.97×10^{-10}
TS3	122.58	4.74	581.40	5.181	26.85	2.06	3.04×10^{-09}	2.21×10^{-08}

As shown in Table 2, as the shell thickness increases around the core, the E_o and E_d values increase. These values can be used to determine n_0 (static-refractive index), ε_s (static-dielectric constant), and f (optical-oscillator strengths) for optical transitions, which are calculated according to the following relations [68];

$$at\ h\upsilon = 0 \rightarrow\ n_0 = \sqrt{1+\frac{E_d}{E_0}} \qquad (10)$$

$$\varepsilon_s = n_0^2 \qquad (11)$$

$$f = E_d E_0 \qquad (12)$$

The calculated values of n_0, ε_s, and f are extracted in Table 2. As the thickness of the shell increases, n_0, ε_s, and f values increase.

The nonlinear parameters like; first- ($\chi^{(1)}$), third- ($\chi^{(3)}$) order nonlinear optical susceptibility, and nonlinear refractive index (n_2) were evaluated as follows [79];

$$\chi^{(1)} = \frac{E_d}{4\pi E_o} \quad (13)$$

$$\chi^{(3)} = 6.82 \times 10^{-15} \left[\frac{E_d}{E_o}\right]^4 \quad (14)$$

$$n_2 = \frac{12\pi\chi^{(3)}}{n_o} \quad (15)$$

Table 2 summarizes the calculated values. From Table 2, as the shell thickness increases, the $\chi^{(1)}$, $\chi^{(3)}$, and n_2 values increase. The $\chi^{(3)}$ value for pure TiO_2 NPs is about 2.08×10^{-14} increases to about 3.04×10^{-09} for core-shell TS3 sample. This value is better than that represented for TiO_2/ZnO thin film ($3.97\text{x}10^{-12}$) [80]. The core-shell TiO_2@SiO_2 structure is the perfect choice for photonic and nonlinear optical devices due to its improved nonlinear optical parameter. A high nonlinear refractive index can be used in communication fibers and optical limiting devices.

The n_2 value increases as the n value increases and E_g decreases, directly correlating with an increase in metallicity. A correlation between the energy gap of oxides and their molar refraction was suggested by Duffy and Lorentz–Lorentz equations as follows [80-82];

$$E_g = 20(1 - \frac{R_m}{V_m})^2 \quad (16)$$

$$1 - \frac{R_m}{V_m} = \left(\frac{E_g}{20}\right)^{\frac{1}{2}} = 1 - \frac{n_o^2-1}{n_o^2+2} \quad (17)$$

where R_m and V_m are the molar refraction and volume, respectively. The value of metallization criterion ($1\text{-}R_m/V_m$) was calculated based on E_g and n_o values and summarized in Table 3.

Table 3: Metallization criterion values.

Sample ID	$\left(\frac{E_g}{20}\right)^{\frac{1}{2}}$	$1 - \frac{n_o^2 - 1}{n_o^2 + 2}$
TiO_2	0.45	0.69
TS1	0.42	0.41
TS2	0.41	0.24
TS3	0.40	0.10

The metallization criterion of TiO_2 NPs is about 0.45, which is near the value in the literature (0.39) [81]. This is due to the difference in bandgap associated with the tiny size of the as-prepared TiO_2. The metallization criterion value decreases with increasing the shell thickness. The width of both valence and conduction bands becomes large when the R_m/V_m value is high, resulting in a narrow band gap and increasing the metallicity of the material [80, 81]. These values provide a solid foundation for anticipating novel nonlinear optical materials.

4. Conclusion

TiO_2 and core-shell $TiO_2@SiO_2$ were synthesized utilizing sol-gel and Stöber methods. The shell thickness was controlled by controlling TEOS concentration during the reaction process. XRD showed that the crystallinity of TiO_2 decreased upon encapsulation with an amorphous silica shell and became more amorphous as the shell thickness increased. TEM analysis confirms the formation of the core-shell $TiO_2@SiO_2$ with different shell thicknesses. TiO_2 nanoparticle absorption increases by encapsulation with a silica shell and increases as the shell thickness increases. The absorbance of the $TiO_2@SiO_2$ nanocomposite can be adjusted by varying the silica shell thickness. It is imperative to adjust this parameter for optimum results. The investigation showed that as the shell thickness increases, the refractive index, optical dielectric constants, and optical conductivity increase, while the optical bandgap and metallization criterion decrease. The core-shell $TiO_2@SiO_2$ structure is the perfect choice for photonic and nonlinear optical devices due to its improved nonlinear optical parameter.

5. References

[1] Park, Wooram, et al. "Advanced hybrid nanomaterials for biomedical applications." Progress in Materials Science 114 (2020): 100686.

[2] Domingues, Joana M., et al. "Nanoparticle Synthesis and Their Integration into Polymer-Based Fibers for Biomedical Applications." Biomedicines 11.7 (2023): 1862.

[3] Abbasi, Reza, et al. "Structural parameters of nanoparticles affecting their toxicity for biomedical applications: a review." Journal of Nanoparticle Research 25.3 (2023): 43.

[4] Ahmed, Hafiz, et al. "Biomedical applications of mesoporous silica nanoparticles as a drug delivery carrier." Journal of Drug Delivery Science and Technology (2022): 103729.

[5] Xia, Changlei, et al. "Optimistic and possible contribution of nanomaterial on biomedical applications: A review." Environmental Research (2022): 114921.

[6] Mahmoudpour, Mansour, et al. "Aptamer functionalized nanomaterials for biomedical applications: Recent advances and new horizons." Nano Today 39 (2021): 101177.

[7] Tsamos, Dimitris, et al. "An Overview of the Production of Magnetic Core-Shell Nanoparticles and Their Biomedical Applications." Metals 12.4 (2022): 605.

[8] Spoială, Angela, et al. "Magnetite-silica core-shell nanostructures: From surface Functionalization towards biomedical applications—a review." Applied Sciences 11.22 (2021): 11075.

[9] Jenjob, Ratchapol, Treethip Phakkeeree, and Daniel Crespy. "Core–shell particles for drug-delivery, bioimaging, sensing, and tissue engineering." *Biomaterials Science* 8.10 (2020): 2756-2770.

[10] Fan, Mingliang, and Minxing Jiang. "Core-shell nanotherapeutics with leukocyte membrane camouflage for biomedical applications." Journal of Drug Targeting 28.9 (2020): 873-881.

[11] dos Santos Batista, Giovanni, Antonio Shigueaki Takimi, and Eleani Maria da Costa. "Hardened oil well cement paste modified with TiO2@ SiO2 nanoparticles: Physical and chemical properties." Construction and Building Materials 367 (2023): 130282.

[12] Fu, Ning, Xue-chang Ren, and Jian-xin Wan. "Preparation of Ag-coated SiO2@ TiO2 core-shell nanocomposites and their photocatalytic applications towards phenol and methylene blue degradation." *Journal of Nanomaterials* 2019 (2019): 1-8.

[13] Gschwend, Pascal. Aerosol-made Nanoparticles for Theranostics: Bioimaging, Nanothermometry, and Photothermal Therapy. Diss. ETH Zurich, 2020.

[14] Hu, Yanjie, et al. "Facile flame synthesis and photoluminescent properties of core-shell TiO2/SiO2 nanoparticles." Journal of alloys and compounds 432.1-2 (2007): L5-L9.

[15] de Dicastillo, Carol López, et al. "Antimicrobial effect of titanium dioxide nanoparticles." Antimicrobial Resistance-A One Health Perspective (2020).

[16] Karthikeyan, C., et al. "Recent advances in semiconductor metal oxides with enhanced methods for solar photocatalytic applications." Journal of Alloys and Compounds 828 (2020): 154281.

[17] Hashmi, Syed Salman, et al. "Potentials of phyto-fabricated nanoparticles as ecofriendly agents for photocatalytic degradation of toxic dyes and waste water treatment, risk assessment and probable mechanism." Journal of the Indian Chemical Society 98.4 (2021): 100019.

[18] Pawar, Tushar Janardan, et al. "Surface modification of titanium dioxide." Journal of Materials Science (2023): 1-44.

[19] Alwis, D.D.D.H., U.G. Chandrika, and P. M. Jayaweera. "Photostability of apocarotenoids on surface of TiO2 semiconductor nanoparticles." Journal of Photochemistry and Photobiology A: Chemistry 407 (2021): 113061.

[20] Srinivas, Kavyashree, and Krishna K. Pandey. "Enhancing photostability of wood coatings using titanium dioxide nanoparticles." Wood is good: current trends and future prospects in wood utilization. Springer Singapore, 2017.

[21] Sood, Swati, et al. "Highly effective Fe-doped TiO2 nanoparticles photocatalysts for visible-light driven photocatalytic degradation of toxic organic compounds." Journal of colloid and interface science 450 (2015): 213-223.

[22] Yang, Xi-jia, et al. "Preparation and photocatalytic performance of Cu-doped TiO2 nanoparticles." Transactions of Nonferrous Metals Society of China 25.2 (2015): 504-509.

[23] Nasikhudin, et al. "Study on photocatalytic properties of TiO2 nanoparticle in various pH condition." Journal of Physics: Conference Series. Vol. 1011. IOP Publishing, 2018.

[24] Jallouli, Nabil, et al. "Photocatalytic degradation of paracetamol on TiO2 nanoparticles and TiO2/cellulosic fiber under UV and sunlight irradiation." Arabian journal of Chemistry 10 (2017): S3640-S3645.

[25] Hossain, Ihteaz M., et al. "Scalable processing of low-temperature TiO2 nanoparticles for high-efficiency perovskite solar cells." ACS Applied Energy Materials 2.1 (2018): 47-58.

[26] Hegazy, Aiat, et al. "TiO2 nanoparticles optimized for photoanodes tested in large area Dye-sensitized solar cells (DSSC)." Solar Energy Materials and Solar Cells 153 (2016): 108-116.

[27] Chu, Liang, et al. "Anatase TiO2 nanoparticles with exposed {001} facets for efficient dye-sensitized solar cells." Scientific reports 5.1 (2015): 12143.

[28] Banerjee, Dipanjan, et al. "Plasmon-enhanced ultrafast and tunable thermo-optic nonlinear optical properties of femtosecond laser ablated TiO2 and Silver-doped TiO2 nanoparticles." Applied Surface Science 569 (2021): 151070.

[29] Seetharaman, Amreetha, et al. "Tunable nanosecond and femtosecond nonlinear optical properties of C–N–S-doped TiO2 nanoparticles." The Journal of Physical Chemistry C 121.43 (2017): 24192-24205.

[30] Dong, Li, et al. "Enhanced broadband nonlinear optical response of TiO2/CuO nanosheets via oxygen vacancy engineering." Nanophotonics 10.5 (2021): 1541-1551.

[31] Karimipour, M., et al. "Synthesis of Ag@ TiO2 core-shells using a rapid microwave irradiation and study of their nonlinear optical properties." Optical Materials 57 (2016): 257-263.

[32] Amanulla, A. Mobeen, and R. J. M. T. P. Sundaram. "Green synthesis of TiO2 nanoparticles using orange peel extract for antibacterial, cytotoxicity and humidity sensor applications." Materials Today: Proceedings 8 (2019): 323-331.

[33] Shetti, Nagaraj P., et al. "Fabrication of MWCNTs and Ru doped TiO2 nanoparticles composite carbon sensor for biomedical application." ECS Journal of Solid State Science and Technology 7.7 (2018): Q3070.

[34] Singh, Preeti, et al. "Highly sensitive ethanol sensor based on TiO2 nanoparticles and its photocatalyst activity." Optik 182 (2019): 512-518.

[35] Gao, Lei, et al. "Facile synthesis of the composites of polyaniline and TiO2 nanoparticles using self-assembly method and their application in gas sensing." Nanomaterials 9.4 (2019): 493.

[36] G. Carturan, R. Dal Toso, S. Boninsegna and R. Dal Monte, “Encapsulation of functional cells by sol–gel silica: actual progress and perspectives for cell therapy”, J. Mater. Chem. 14 (2004) 2087.

[37] Son, Suim, et al. "Designed synthesis of SiO2/TiO2 core/shell structure as light scattering material for highly efficient dye-sensitized solar cells." *ACS applied materials & interfaces* 5.11 (2013): 4815-4820.

[38] Zhang, Ruifang, Fei Yan, and Yu Chen. "Exogenous physical irradiation on titania semiconductors: Materials chemistry and tumor□specific nanomedicine." Advanced Science 5.12 (2018): 1801175.

[39] Çeşmeli, Selin, and Cigir Biray Avci. "Application of titanium dioxide (TiO2) nanoparticles in cancer therapies." Journal of drug targeting 27.7 (2019): 762-766.

[40] Feng, Xiaohui, Shaokun Zhang, and Xia Lou. "Controlling silica coating thickness on TiO2 nanoparticles for effective photodynamic therapy." *Colloids and Surfaces B: Biointerfaces* 107 (2013): 220-226.

[41] Albukhaty, Salim, et al. "Preparation and characterization of titanium dioxide nanoparticles and in vitro investigation of their cytotoxicity and antibacterial activity against Staphylococcus aureus and Escherichia coli." Animal Biotechnology 33.5 (2022): 864-870.

[42] Hashem, Murtaza, and Hassan Al-Karagoly. "Synthesis, characterization, and cytotoxicity of titanium dioxide nanoparticles and in vitro study of its impact on lead concentrations in bovine blood and milk." Journal of Biotech Research 12 (2021).

[43] Gonçalves, M. Clara. "Sol-gel silica nanoparticles in medicine: A natural choice. Design, synthesis and products." *Molecules* 23.8 (2018): 2021.

[44] Kumar, Pawan, et al. "Highly luminescent biocompatible CsPbBr 3@ SiO 2 core–shell nanoprobes for bioimaging and drug delivery." Journal of Materials Chemistry B 8.45 (2020): 10337-10345.

[45] Adamska, E., et al. "Characterization and Cytotoxicity Comparison of Silver-and Silica-Based Nanostructures. Materials 2021, 14, 4987." (2021).

[46] Singh, Th Nando, Th Gomti Devi, and Sh Dorendrajit Singh. "Synthesis, characterization and optical study of lanthanide activated TiO2@ SiO2 core–shell nanoparticle." Nano-Structures & Nano-Objects 10 (2017): 182-191.

[47] Slomberg, Danielle L., et al. "Release and fate of nanoparticulate TiO2 UV filters from sunscreen: Effects of particle coating and formulation type." Environmental Pollution 271 (2021): 116263.

[48] Swain, Basudev, et al. "Synthesis of cosmetic grade TiO2-SiO2 core-shell powder from mechanically milled TiO2 nanopowder for commercial mass production." Materials Science and Engineering: C 95 (2019): 95-103.

[49] Leong, Hui Jun, and Seong-Geun Oh. "Preparation of antibacterial TiO2 particles by hybridization with azelaic acid for applications in cosmetics." Journal of Industrial and Engineering Chemistry 66 (2018): 242-247.

[50] Feng, X., Zhang, S., & Lou, X. (2013). Controlling silica coating thickness on TiO2 nanoparticles for effective photodynamic therapy. Colloids and Surfaces B: Biointerfaces, 107, 220-226.

[51] Bai, Yali, et al. "Higher UV-shielding ability and lower photocatalytic activity of TiO 2@ SiO 2/APTES and its excellent performance in enhancing the photostability of poly (p-phenylene sulfide)." RSC advances 7.35 (2017): 21758-21767.

[52] Feng, Xiaohui, et al. "A novel folic acid-conjugated TiO2–SiO2 photosensitizer for cancer targeting in photodynamic therapy." Colloids and Surfaces B: Biointerfaces 125 (2015): 197-205.

[53] Shen, Qing, and Hon-Yeung Cheung. "TiO2/SiO2 core–shell composite-based sample preparation method for selective extraction of phospholipids from shrimp waste followed by hydrophilic interaction chromatography coupled with quadrupole time-of-flight/mass spectrometry analysis." Journal of agricultural and food chemistry 62.36 (2014): 8944-8951.

[54] Kupriyanov, Artem Nikolaevich, et al. "Synthesis and Research of Nanocompositions of Oxide Materials Based on Titanium Dioxide for use as Contrast Agents in Optical Coherence Tomography." Journal of Pharmaceutical Research International 33.40A (2021): 325-338.

[55] Tauc, J., Radu Grigorovici, and Anina Vancu. "Optical properties and electronic structure of amorphous germanium." physica status solidi (b) 15.2 (1966): 627-637.

[56] Xu, Zili, et al. "Structure, luminescence properties and photocatalytic activity of europium doped-TiO 2 nanoparticles." Journal of materials science 40.6 (2005): 1539-1541.

[57] Wang, Fangke, et al. "Structural Design for Controlling the Lattice Strain Relaxation Process in TiO2/SiO2 Core–Shell Nanoparticles." *ACS Sustainable Chemistry & Engineering* 9.49 (2021): 16796-16807.

[58] Shilova, Olga A., et al. "Surface and photocatalytic properties of sol–gel derived TiO2@ SiO2 core-shell nanoparticles." *Journal of Sol-Gel Science and Technology* (2022): 1-11.

[59] Samangsri, Suwapee, Thanita Areerob, and Siriluk Chiarakorn. "Core-shell Nitrogen-Doped TiO2@ SiO2 Nano-Catalyst as an Additive in Photocatalytic Paint for Gaseous Acetaldehyde Decomposition." Catalysts 13.2 (2023): 351.

[60] Sun, Jinfeng, et al. "Influence of core-shell TiO2@ SiO2 nanoparticles on cement hydration." Construction and Building Materials 156 (2017): 114-122.

[61] Wang, Xiaoman, and Hongling Chen. "A new approach to preparation of TiO2@ void@ SiO2 rattle type core shell structure nanoparticles via titanyl oxalate complex." Colloids and Surfaces A: Physicochemical and Engineering Aspects 485 (2015): 25-33.

[62] Cabezuelo, Oscar, et al. "Optimizing the use of light in supported TiO2 photocatalysts: Relevance of the shell thickness." Journal of Photochemistry and Photobiology A: Chemistry (2023): 114917.

[63] Xu, Guangqing, et al. "Effect of silica on the microstructure and photocatalytic properties of titania." Ceramics International 35.1 (2009): 1-5.

[64] Zhang, Xin, Feng Zhang, and Kwong-Yu Chan. "Synthesis of titania–silica mixed oxide mesoporous materials, characterization and photocatalytic properties." Applied Catalysis A: General 284.1-2 (2005): 193-198.

[65] Ogura, K., et al. "Thermogravimetry/mass spectrometry of urease-immobilized sol–gel silica and the application of such a urease-modified electrode to the potentiometric determination of urea." Analytica chimica acta 384.2 (1999): 219-225.

[66] Li, Zhijie, et al. "Comparative study of sol–gel-hydrothermal and sol–gel synthesis of titania–silica composite nanoparticles." Journal of Solid State Chemistry 178.5 (2005): 1395-1405.

[67] Gao, Shuyan, et al. "Enhanced electromechanical property of silicone elastomer composites containing TiO2@ SiO2 core-shell nano-architectures." Polymers 13.3 (2021): 368.

[68] Khalid, A., et al., Fe3O4 nanoparticles and Fe3O4@ SiO2 core-shell: synthesize, structural, morphological, linear, and nonlinear optical properties. Journal of Alloys and Compounds, 2023. 947: p. 169639.

[69] Qutub, N., et al., *Enhanced photocatalytic degradation of Acid Blue dye using CdS/TiO2 nanocomposite.* Scientific Reports, 2022. **12**(1): p. 5759.

[70] Chougala, L., et al., A simple approach on synthesis of TiO2 nanoparticles and its application in dye sensitized solar cells. 2017.

[71] J. Singh, Optical Properties of Condensed Matter and Applications, JohnWiley & Sons Inc., 2019.

[72] S. Wang, L.N. Bai, H.M. Sun, Q. Jiang, J.S. Lian, Structure and photocatalytic property of Mo-doped TiO2 nanoparticles, Powder Technol. 244 (2013) 9–15.

[73] Alamgir, W. Khan, S. Ahmad, M. Mehedi Hassan, A.H. Naqvi, Structural phase analysis, band gap tuning and fluorescence properties of Co doped TiO2 nanoparticles, Opt. Mater. (Amst). 38 (2014) 278–285.

[74] N. G., D.R. A., A.I. A., J. R.L., Tuning the optical band Gap of pure TiO2 via photon induced method, Optik (Stuttg). 179 (2019) 889–894.

[75] Y. Zhao, C. Li, X. Liu, F. Gu, H. Jiang, W. Shao, L. Zhang, Y. He, Synthesis and optical properties of TiO2 nanoparticles, Mater. Lett. 61 (2007) 79–83.

[76] S.A. Mahmoud, A.A. Akl, S.M. Al-shomar, Effect of some preparative parameters on optical properties of spray deposited iridium oxide thin films, Phys. B. 404 (2009) 2151–2158.

[77] A.S. Hassanien, A.A. Akl, Influence of composition on optical and dispersion parameters of thermally evaporated non-crystalline Cd50S50-xSex thin films, J. Alloys Compd. 648 (2015) 280–290.

[78] H.E. Atyia, N.A. Hegab, Optical spectroscopy and dispersion parameters of Ge15Se60X25 (X = As or Sn) amorphous thin films, Eur. Phys. J. Appl. Phys. 63 (2013) 10301.

[79] Alshahrani, H.I. Elsaeedy, A.H. Korna, H.A. Yakout, A.H. Ashour, A.A. Maksoud, R. Amer, A.S. Awed, Revealing the effect of gamma irradiation on structural, ferromagnetic resonance, optical, and dispersion properties of PVC/Mn 0 . 5 Zn 0.5 Fe2O4 nanocomposite films, Opt. Mater. (Amst). 118 (2021) 111216.

[80] S.S. Fouad, B. Parditka, A.E. Bekheet, H.E. Atyia, Z. Erdélyi, ALD of TiO2/ZnO mutilayers towards the understanding of optical properties and polarizability, Opt. Laser Technol. 140 (2021).

[81] V. Dimitrov, S. Sakka, Linear and nonlinear optical properties of simple oxides. II, J. Appl. Phys. 79 (1996) 1741–1745.

[82] M.K. Halimah, M.F. Faznny, M.N. Azlan, H.A.A. Sidek, Optical basicity and electronic polarizability of zinc borotellurite glass doped La3+ ions, Results Phys. 7 (2017) 581–589.

Declaration of interests

☒ The authors declare that they have no known competing financial interests or personal relationships that could have appeared to influence the work reported in this paper.

☐The authors declare the following financial interests/personal relationships which may be considered as potential competing interests: